PROCEEDINGS OF THE ROYAL SOCIETY A

Proc. R. Soc. A (2006) **462**, 149–169
doi:10.1098/rspa.2005.1566
Published online 9 November 2005

The *N*-vortex problem on a rotating sphere. I Multi-frequency configurations

By Paul K. Newton* and Houman Shokraneh

Department of Aerospace & Mechanical Engineering and Department of Mathematics, University of Southern California, Los Angeles, CA 90089-1191, USA

The problem of *N*-point vortices moving on a rotating unit sphere is considered. Through a sequence of linear coordinate transformations, which takes into account the orientation of the centre of vorticity vector with respect to the axis of rotation, we show how to reduce the problem to that on a non-rotating sphere, where the centre of vorticity vector is aligned with the z-axis. As a consequence, we prove that integrability on the rotating sphere is the same as on the non-rotating sphere, namely, the three-vortex problem on the rotating sphere is integrable for all vortex strengths, while the four-vortex problem is integrable in the special case where the centre of vorticity is zero. Rigid multi-frequency configurations that retain their shape while rotating about two independent axes with two independent frequencies are obtained, and necessary conditions for one- and two-frequency motions are derived. Examples including dipoles which exhibit global 'wobbling' and 'tumbling' dynamics, rings, and Platonic solid configurations are shown to undergo either periodic or quasi-periodic evolution on the rotating sphere depending on the ratio of the solid-body rotational frequency Ω to the rotational frequency ω associated with the rigid structure.

Keywords: *N*-vortex problem; multi-frequency solutions; rotating sphere; integrable systems

1. Introduction

In this paper, we consider the *N*-vortex problem on a rotating unit sphere. It is convenient to formulate the problem in Cartesian coordinates, where the vector $\boldsymbol{x}_\alpha \in \mathbb{R}^3$ points from the centre of the unit sphere to the point vortex with strength $\Gamma_\alpha \in \mathbb{R}$ lying in the surface of the sphere, as shown in figure 1. Each point vortex moves under the collective influence of all the others and rotation is introduced by adding a solid-body rotational component to the velocity field. The dynamical system we consider is given by

$$\left.\begin{aligned} \dot{\boldsymbol{x}}_\alpha &= \frac{1}{4\pi}\sum_{\beta=1}^{N}{}' \Gamma_\beta \frac{\boldsymbol{x}_\beta \times \boldsymbol{x}_\alpha}{(1-\boldsymbol{x}_\alpha\cdot\boldsymbol{x}_\beta)} + \Omega\hat{\boldsymbol{e}}_z \times \boldsymbol{x}_\alpha, \quad \alpha = 1,\ldots,N, \\ \boldsymbol{x}_\alpha &\in \mathbb{R}^3, \quad ||\boldsymbol{x}_\alpha|| = 1. \end{aligned}\right\} \tag{1.1}$$

* Author for correspondence (newton@spock.usc.edu).

Received 21 October 2004
Accepted 11 August 2005

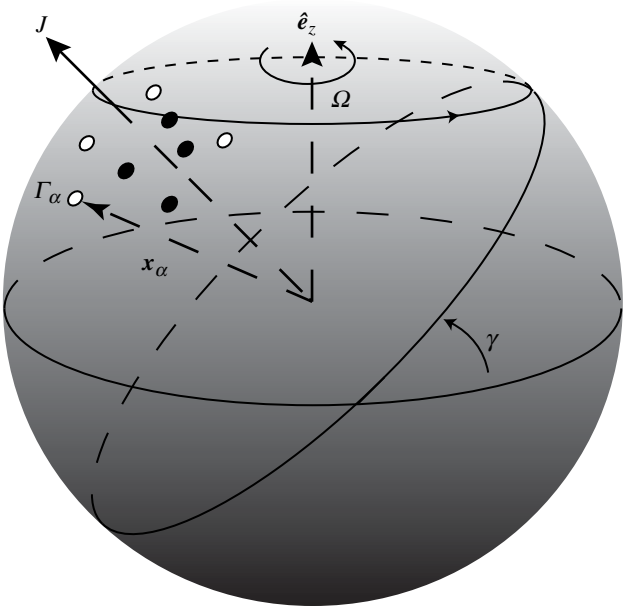

Figure 1. N-vortex diagram on a unit rotating sphere. $\boldsymbol{J}$ rotates around $\hat{\boldsymbol{e}}_z$ with frequency Ω.

The prime on the summation reminds us that the singular term $\beta=\alpha$ is omitted and initially, the vortices are located at the given positions $\boldsymbol{x}_\alpha(0)\in\mathbb{R}^3$, $\alpha=1, \ldots, N$. The denominator in (1.1) is the chord distance between vortex Γ_α and Γ_β, since $\|\boldsymbol{x}_\alpha-\boldsymbol{x}_\beta\|^2=2(1-\boldsymbol{x}_\alpha\cdot\boldsymbol{x}_\beta)$. In what follows, the *centre of vorticity* vector $\boldsymbol{J}$ (also known as the momentum map), defined as

$$\boldsymbol{J}=\sum_{\alpha=1}^{N}\Gamma_\alpha\boldsymbol{x}_\alpha=\left(\sum_{\alpha=1}^{N}\Gamma_\alpha x_\alpha,\sum_{\alpha=1}^{N}\Gamma_\alpha y_\alpha,\sum_{\alpha=1}^{N}\Gamma_\alpha z_\alpha\right)=(J_x,J_y,J_z), \tag{1.2}$$

plays a central role in our discussion.

There is, by now, a substantial and growing literature devoted to the N-vortex problem on the non-rotating sphere ($\Omega=0$) and much is known regarding integrability (see Borisov & Lebedev 1998; Borisov & Pavlov 1998; Kidambi & Newton 1998, 2000) non-integrability (see Bagrets & Bagrets 1997) collisions (see Kidambi & Newton 1998, 1999), fixed and relative equilibria (see Kidambi & Newton 1998; Lim *et al.* 2001; Laurent-Polz 2002*a*,*b*; Aref *et al.* 2003), and stability (see Polvani & Dritschel 1993; Pekarsky & Marsden 1998; Cabral *et al.* 2003; Kurakin 2004; Laurent-Polz *et al.* 2004). Monte-Carlo methods have been developed which identify extremal states (see Lim *et al.* 2003*a*,*b*) and special numerical techniques that retain accuracy on theoretically conserved quantities are being developed (Pullin & Saffman 1991; Zhang & Qin 1993; Marsden *et al.* 1999; Newton & Khushalani 2002; Rowley & Marsden 2002; Rowley *et al.* 2004). An overview of many of these topics can be found in Newton (2001), while a recent comprehensive survey of equilibrium configurations can be found in Aref *et al.* (2003). What motivates most of these efforts are applications to atmospheric flows, traditionally treated under the β-plane approximation (see Gill 1982). While β-plane models include Coriolis effects, they are local

and only remain valid in a restricted latitudinal strip about which the tangent plane approximation is invoked. Thus, when one is interested in tracking vorticity over long distances, or when global velocity fields and streamline patterns are of interest (Kidambi & Newton 2000) typically a full spherical treatment is required. The problem has spawned several Ph.D. theses, both from the geophysical fluid dynamics perspective (see Chern 1991; Neven 1993; DiBattista 1997) as well as the nonlinear dynamics point of view (see Kidambi 1999; Jamaloodeen 2000; Laurent-Polz 2002*a*,*b*; Nebus 2003; Khushalani 2004).

The papers of Bogomolov (1985), Klyatskin & Reznik (1989) and DiBattista & Polvani (1998) treat the fully coupled 'barotropic' model on the sphere, where the vortices influence the background rotation and in turn, the evolving background field influences the vortices. This two-way coupling allows for the generation of Rossby–Haurwitz waves on the sphere which are known, for example, to trigger instabilities in the vortex configuration. However, because the background vorticity is not localized, Bogomolov's (1985) equations are integro-differential equations which typically must be treated numerically. Likewise, Klyatskin & Reznik (1989) resort to use a short-time approximation (Taylor expansion) to show that an isolated point vortex, coupled to the background field, moves along a northwesterly curved trajectory on the sphere, in qualitative agreement with what is known about the trajectories of hurricane paths in the Northern Hemisphere. The numerical study in DiBattista & Polvani (1998) treats the interaction of a vortex dipole with a background distribution in the form of constant vorticity strips on the sphere which initially model solid-body rotation, while Polvani & Dritschel (1993) treats both wave and vortex dynamics on the sphere using contour dynamics techniques. In our simpler model, since the vortex motion does not affect the background velocity field, which remains in solid-body form, the system retains its finite-dimensional structure, much like the models that focus on the non-rotating sphere and thus can be treated analytically. Our model can be considered a limiting case of the two-way coupled model in the limit in which the background field is strong compared to the strength of the embedded vortices. The price we pay is that this one-way coupled system is not capable of generating Rossby–Haurwitz waves.

Our goal in this paper is to make a simple observation that seems to have been missed previously. Namely, that the misalignment of the centre of vorticity vector with the axis of rotation is an important ingredient in understanding the dynamics of the vortices, and on its own can account for features such as the 'wobbling' and 'tumbling' modes seen previously in β-plane models (see §5). The key to understanding the ramifications of the misalignment is to understand how a certain time-dependent unitary operator, $\mathcal{L}_{\mathcal{Q}}^{\boldsymbol{J}}(t)$, affects trajectories on the aligned non-rotating sphere. It is this feature that we will explore in this paper.

In §2, we transform system (1.1) to the corresponding equations for N-vortices on a non-rotating sphere. In §3, we align the $\boldsymbol{J}$ vector with the z-axis through two sequential linear transformations. We show that the general solution to (1.1) can be related, via a sequence of three linear mappings which define $\mathcal{L}_{\mathcal{Q}}^{\boldsymbol{J}}(t)$, to solutions on the non-rotating sphere, where $\boldsymbol{J}$ is aligned with the z-axis. From this, we can conclude that, like the non-rotating sphere (Kidambi & Newton 1998), the three-vortex problem on the rotating sphere is integrable for all vortex strengths. This is described in §4. Section 5 focuses on the conditions necessary for the existence of rigidly rotating configurations which maintain the mutual

distances between each pair of vortices on the rotating sphere. These solutions contain two inherent frequencies (Ω, ω) and hence represent either periodic orbits (Ω/ω rational) or quasi-periodic orbits (Ω/ω irrational) of the original system (1.1). We then describe the evolution of dipoles, rings and Platonic solid configurations on the rotating sphere. In a companion paper (part II), we will describe the Hamiltonian formulation for this system.

(*a*) *Solid-body rotation*

Consider first, just the solid-body term in (1.1):

$$\left.\begin{aligned} &\dot{\boldsymbol{x}} = \Omega \hat{\boldsymbol{e}}_z \times \boldsymbol{x} = (-\Omega y, \Omega x, 0), \\ &\boldsymbol{x} \in \mathbb{R}^3, \quad \|\boldsymbol{x}\| = 1. \end{aligned}\right\} \tag{1.3}$$

(1.3) can be solved by transforming the coordinates to a rotating reference frame via the linear transformation $\boldsymbol{x} \in \mathbb{R}^3 \mapsto \boldsymbol{w} \in \mathbb{R}^3$, where

$$\boldsymbol{x} = \boldsymbol{M}_\Omega \boldsymbol{w}, \tag{1.4}$$

where $\boldsymbol{M}_\Omega$ is the rotation matrix about the z-axis:

$$\boldsymbol{M}_\Omega = \begin{pmatrix} \cos \Omega t & -\sin \Omega t & 0 \\ \sin \Omega t & \cos \Omega t & 0 \\ 0 & 0 & 1 \end{pmatrix}. \tag{1.5}$$

For future reference, we note that $\boldsymbol{M}_\Omega(0) = \boldsymbol{I}$ and that $\boldsymbol{M}_\Omega$ is a unitary matrix, hence has the property

$$\boldsymbol{M}_\Omega^{\mathrm{T}} = \boldsymbol{M}_\Omega^{-1}. \tag{1.6}$$

Inserting this into (1.3) yields

$$\dot{\boldsymbol{x}} = \dot{\boldsymbol{M}}_\Omega \boldsymbol{w} + \boldsymbol{M}_\Omega \dot{\boldsymbol{w}} = \Omega \hat{\boldsymbol{e}}_z \times (\boldsymbol{M}_\Omega \boldsymbol{w}). \tag{1.7}$$

A straightforward calculation shows that

$$\dot{\boldsymbol{M}}_\Omega \boldsymbol{w} = \Omega \hat{\boldsymbol{e}}_z \times (\boldsymbol{M}_\Omega \boldsymbol{w}) = \Omega \hat{\boldsymbol{e}}_z \times \boldsymbol{x}. \tag{1.8}$$

Thus, (1.7) reduces to

$$\boldsymbol{M}_\Omega \dot{\boldsymbol{w}} = 0 \Rightarrow \boldsymbol{w} = \boldsymbol{w}(\boldsymbol{0}) = \boldsymbol{x}(\boldsymbol{0}), \tag{1.9}$$

and the solution to (1.3) then becomes

$$\boldsymbol{x}(t) = \boldsymbol{M}_\Omega \boldsymbol{x}(0). \tag{1.10}$$

(*b*) *The centre of vorticity vector*

Central to our approach is the centre of vorticity vector (1.2), in particular its orientation with respect to the axis of rotation. We first consider its evolution

equation by multiplying (1.1) by Γ_α and summing over α:

$$\sum_{\alpha=1}^{N}\Gamma_\alpha\dot{\boldsymbol{x}}_\alpha=\sum_{\alpha=1}^{N}{\sum_{\beta=1}^{N}}'\Gamma_\alpha\Gamma_\beta\frac{\boldsymbol{x}_\beta\times\boldsymbol{x}_\alpha}{(1-\boldsymbol{x}_\alpha\cdot\boldsymbol{x}_\beta)}+\sum_{\alpha=1}^{N}\Omega\hat{\boldsymbol{e}}_z\times\Gamma_\alpha\boldsymbol{x}_\alpha, \tag{1.11}$$

$$=\Omega\hat{\boldsymbol{e}}_z\times\sum_{\alpha=1}^{N}\Gamma_\alpha\boldsymbol{x}_\alpha. \tag{1.12}$$

Thus, $\boldsymbol{J}$ satisfies

$$\dot{\boldsymbol{J}}=\Omega\hat{\boldsymbol{e}}_z\times\boldsymbol{J}, \tag{1.13}$$

the same equation as (1.3). Hence, as in (1.10),

$$\boldsymbol{J}(t)=\boldsymbol{M}_\Omega\boldsymbol{J}(0), \tag{1.14}$$

from which we conclude that its length is constant since

$$\|\boldsymbol{J}\|^2=\langle\boldsymbol{J},\boldsymbol{J}\rangle=\langle\boldsymbol{M}_\Omega\boldsymbol{J}(0),\boldsymbol{M}_\Omega\boldsymbol{J}(0)\rangle=\langle\boldsymbol{M}_\Omega^{\mathrm{T}}\boldsymbol{M}_\Omega\boldsymbol{J}(0),\boldsymbol{J}(0)\rangle=\|\boldsymbol{J}(0)\|^2. \tag{1.15}$$

The components satisfy

$$J_x^2+J_y^2=C_1=\text{const.}, \tag{1.16}$$

$$J_z=C_2=\text{const.} \tag{1.17}$$

A general configuration is depicted in figure 1. As the N-vortices evolve under their mutual interaction, the $\boldsymbol{J}$ vector rotates with frequency Ω about the z-axis, maintaining a fixed angle γ with respect to the axis.

2. Transformation to a non-rotating sphere

To treat the full system (1.1), we first move to a rotating reference frame to absorb the solid-body rotational term, hence substitute (1.4) into (1.1). Noting that

$$\boldsymbol{x}_\alpha\cdot\boldsymbol{x}_\beta=\langle\boldsymbol{x}_\alpha,\boldsymbol{x}_\beta\rangle=\langle\boldsymbol{M}_\Omega\boldsymbol{w}_\alpha,\boldsymbol{M}_\Omega\boldsymbol{w}_\beta\rangle \tag{2.1}$$

$$=\langle\boldsymbol{M}_\Omega^{\mathrm{T}}\boldsymbol{M}_\Omega\boldsymbol{w}_\alpha,\boldsymbol{w}_\beta\rangle=\langle\boldsymbol{w}_\alpha,\boldsymbol{w}_\beta\rangle \tag{2.2}$$

and that

$$\boldsymbol{x}_\alpha\times\boldsymbol{x}_\beta=(\boldsymbol{M}_\Omega\boldsymbol{w}_\alpha)\times(\boldsymbol{M}_\Omega\boldsymbol{w}_\beta)=\boldsymbol{M}_\Omega(\boldsymbol{w}_\alpha\times\boldsymbol{w}_\beta), \tag{2.3}$$

we obtain

$$\dot{\boldsymbol{w}}_\alpha=\frac{1}{4\pi}{\sum_{\beta=1}^{N}}'\Gamma_\beta\frac{\boldsymbol{w}_\beta\times\boldsymbol{w}_\alpha}{(1-\boldsymbol{w}_\alpha\cdot\boldsymbol{w}_\beta)},\quad \boldsymbol{w}_\alpha(0)=\boldsymbol{x}_\alpha(0),\quad \alpha=1,\ldots,N. \tag{2.4}$$

Hence, transformation (1.4) takes solutions on the rotating sphere to solutions on the non-rotating sphere. The centre of vorticity vector transforms as

$$\boldsymbol{J}=\sum_{\alpha=1}^{N}\Gamma_\alpha\boldsymbol{x}_\alpha=\sum_{\alpha=1}^{N}\Gamma_\alpha\boldsymbol{M}_\Omega\boldsymbol{w}_\alpha=\boldsymbol{M}_\Omega\sum_{\alpha=1}^{N}\Gamma_\alpha\boldsymbol{w}_\alpha=\boldsymbol{M}_\Omega\hat{\boldsymbol{J}}, \tag{2.5}$$

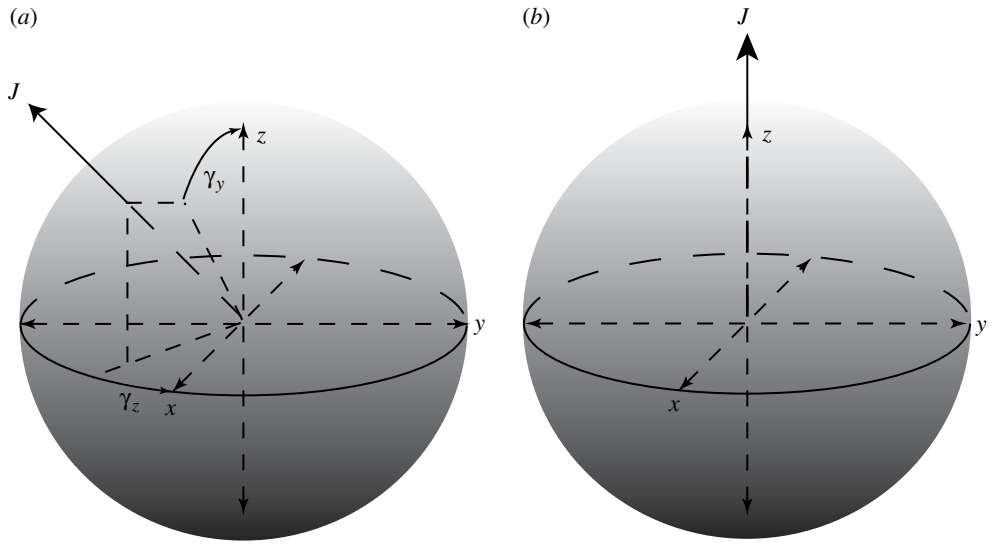

Figure 2. Alignment of $\boldsymbol{J}$ with the $\hat{\boldsymbol{e}}_z$-axis is obtained via a rotation through angle γ_z about the z-axis followed by a rotation through angle γ_y about the y-axis.

where

$$\hat{\boldsymbol{J}} = \sum_{\alpha=1}^{N} \Gamma_\alpha \boldsymbol{w}_\alpha = (\hat{J}_x, \hat{J}_y, \hat{J}_z) = \boldsymbol{J}(0) = \text{const.} \tag{2.6}$$

The initial configuration $\boldsymbol{w}_\alpha(0) = \boldsymbol{x}_\alpha(0)$, $\alpha = 1, \ldots, N$ defines the constant vector $\hat{\boldsymbol{J}}$.

3. Alignment

We now rotate $\hat{\boldsymbol{J}}$, so that it is aligned with the z-axis as shown in figure 2. First, we multiply by the matrix $\boldsymbol{M}_z$ which rotates $\hat{\boldsymbol{J}}$ around the z-axis so that it lies in the (x, z) plane, then we multiply by $\boldsymbol{M}_y$ which rotates the vector around the y-axis. Hence

$$\boldsymbol{M}_y \boldsymbol{M}_z \tilde{\boldsymbol{J}} \equiv \tilde{\boldsymbol{J}} = (0, 0, \tilde{J}_z), \tag{3.1}$$

where

$$\boldsymbol{M}_z = \begin{pmatrix} \cos\gamma_z & -\sin\gamma_z & 0 \\ \sin\gamma_z & \cos\gamma_z & 0 \\ 0 & 0 & 1 \end{pmatrix}, \tag{3.2}$$

$$\boldsymbol{M}_y = \begin{pmatrix} \cos\gamma_y & 0 & \sin\gamma_y \\ 0 & 1 & 0 \\ -\sin\gamma_y & 0 & \cos\gamma_y \end{pmatrix}. \tag{3.3}$$

Letting $\boldsymbol{z}_\alpha \equiv \boldsymbol{M}_y\boldsymbol{M}_z\boldsymbol{w}_\alpha$, $\boldsymbol{w}_\alpha \equiv (\boldsymbol{M}_y\boldsymbol{M}_z)^{\mathrm{T}}\boldsymbol{z}_\alpha$ gives the aligned system

$$\dot{\boldsymbol{z}}_\alpha = \frac{1}{4\pi}\sum_{\beta=1}^{N}{}' \Gamma_\beta \frac{\boldsymbol{z}_\beta \times \boldsymbol{z}_\alpha}{(1-\boldsymbol{z}_\alpha\cdot\boldsymbol{z}_\beta)}, \quad \boldsymbol{z}_\alpha(0) = \boldsymbol{M}_y\boldsymbol{M}_z\boldsymbol{x}_\alpha(0), \tag{3.4}$$

$$\tilde{\boldsymbol{J}} = \sum_{\alpha=1}^{N}\Gamma_\alpha\boldsymbol{z}_\alpha = (0,0,\tilde{J}_z), \tag{3.5}$$

where

$$\tilde{J}_z = \hat{J}_z = J_z = \text{const.}$$

4. Integrability

The relation between solutions of the original rotating system, $\boldsymbol{x}_\alpha(t)$, and solutions of the aligned system $\boldsymbol{z}_\alpha(t)$, and in some sense the key result of this paper, is via the linear operator $\mathcal{L}^{\boldsymbol{J}}_{\Omega}(t) \equiv \boldsymbol{M}_\Omega(t)\boldsymbol{M}_z^{-1}\boldsymbol{M}_y^{-1}$

$$\boldsymbol{x}_\alpha(t) = \mathcal{L}^{\boldsymbol{J}}_{\Omega}(t)\boldsymbol{z}_\alpha(t). \tag{4.1}$$

This operator is time-dependent, but more importantly contains information on the original alignment of the $\boldsymbol{J}$ vector with the axis of rotation. Central to the question of integrability is the rate of separation of the vortices as measured by $\|\boldsymbol{x}_\alpha-\boldsymbol{x}_\beta\|^2$ on the rotating sphere and $\|\boldsymbol{z}_\alpha-\boldsymbol{z}_\beta\|^2$ on the non-rotating aligned sphere. The two quantities are equal since

$$\begin{aligned}\|\boldsymbol{x}_\alpha-\boldsymbol{x}_\beta\|^2 &= \langle\boldsymbol{x}_\alpha-\boldsymbol{x}_\beta,\boldsymbol{x}_\alpha-\boldsymbol{x}_\beta\rangle = 2(1-\langle\boldsymbol{x}_\alpha,\boldsymbol{x}_\beta\rangle)\\ &= 2(1-\langle\boldsymbol{M}_\Omega(t)\boldsymbol{M}_z^{-1}\boldsymbol{M}_y^{-1}\boldsymbol{z}_\alpha,\boldsymbol{M}_\Omega(t)\boldsymbol{M}_z^{-1}\boldsymbol{M}_y^{-1}\boldsymbol{z}_\beta\rangle)\\ &= 2(1-\langle\boldsymbol{M}_y\boldsymbol{M}_z\boldsymbol{M}_\Omega(t)^{-1}\boldsymbol{M}_\Omega(t)\boldsymbol{M}_z^{-1}\boldsymbol{M}_y^{-1}\boldsymbol{z}_\alpha,\boldsymbol{z}_\beta\rangle) = 2(1-\langle\boldsymbol{z}_\alpha,\boldsymbol{z}_\beta\rangle)\\ &= \|\boldsymbol{z}_\alpha-\boldsymbol{z}_\beta\|^2.\end{aligned}$$

For the aligned non-rotating system, we know from Kidambi & Newton (1998) that the three-vortex problem is integrable for all vortex strengths. From this result and (4.1) follows.

Proposition 4.1 (Integrability on the rotating sphere). *The three-vortex problem on the rotating sphere (1.1) is integrable for all vortex strengths. The four-vortex problem is integrable if the centre of vorticity vector $\boldsymbol{J}=0$. All solutions on the rotating sphere are mapped to solutions on the aligned non-rotating sphere via the linear transformation (4.1).*

The proof for the non-rotating sphere can be found in Borisov & Lebedev (1998), Borisov & Pavlov (1998) and Kidambi & Newton (1998), with discussions in Newton (2001). At first glance, this result is somewhat surprising in view of Noether's theorem and the fact that the rotating problem has one less conserved quantity than the non-rotating problem (e.g. $J_x^2+J_y^2$, J_z compared with J_x, J_y, J_z). However, the proof of integrability for the non-rotating problem relies solely on the conservation of the three independent and involutive quantities $J_x^2+J_y^2$, J_z, as well as the underlying Hamiltonian and never makes use of the fact that J_x and J_y are each conserved.

5. Rigid configurations

We now examine the evolution of *rigid configurations* on the rotating sphere, which we define as those in which distances between each pair of vortices remain fixed, i.e. $\|\boldsymbol{x}_\alpha - \boldsymbol{x}_\beta\|^2 = \text{const}$. Note that since

$$\langle \boldsymbol{x}_\alpha, \boldsymbol{x}_\beta \rangle = \langle \boldsymbol{w}_\alpha, \boldsymbol{w}_\beta \rangle = \langle \boldsymbol{z}_\alpha, \boldsymbol{z}_\beta \rangle \tag{5.1}$$

configurations that are rigid on the non-rotating sphere (aligned or non-aligned) are also rigid on the rotating sphere, hence, in what follows, we will use equation (2.4) to draw conclusions regarding rigid configurations on the rotating sphere. In particular, taking the dot product of (2.6) with $\boldsymbol{w}_\alpha$ along with the condition that $\langle \boldsymbol{w}_\alpha, \boldsymbol{w}_\beta \rangle = \text{const.}$ gives

$$\boldsymbol{w}_\alpha \cdot \hat{\boldsymbol{J}} = \text{const.}, \tag{5.2}$$

i.e. the angle between each vortex and the centre of vorticity vector remains fixed. Next, using system (2.4) along with the *ansatz* that each vortex moves with the same frequency around the same axis, i.e. $\dot{\boldsymbol{w}}_\alpha \equiv \boldsymbol{\omega} \times \boldsymbol{w}_\alpha$, we obtain

$$\boldsymbol{\omega} \times \boldsymbol{w}_\alpha = \frac{1}{4\pi} {\sum_{\beta=1}^{N}}' \Gamma_\beta \frac{\boldsymbol{w}_\beta \times \boldsymbol{w}_\alpha}{(1 - \boldsymbol{w}_\alpha \cdot \boldsymbol{w}_\beta)}. \tag{5.3}$$

Then, multiplying by Γ_α and summing over α gives the condition

$$\boldsymbol{\omega} \times \hat{\boldsymbol{J}} = 0. \tag{5.4}$$

Thus, on the non-rotating sphere, non-degenerate ($\hat{\boldsymbol{J}} \neq 0$) rigid configurations that rotate around the $\hat{\boldsymbol{J}}$-axis with frequency ω move on constant latitudinal planes perpendicular to $\hat{\boldsymbol{J}}$. Hence, on the rotating sphere we have the following.

Proposition 5.1 (Rigid configurations). *Rigid configurations on the rotating sphere that rotate around the $\boldsymbol{J}$-axis with frequency ω move on a constant latitudinal planes perpendicular to $\boldsymbol{J}$. The centre of vorticity vector $\boldsymbol{J}$ rotates around the z-axis with frequency Ω. When $\omega = 0$, the rigid configurations have one frequency Ω, but in general they are made up of two independent frequencies (Ω, ω). The general case is shown in figure 3.*

The one-frequency solutions are *fixed equilibria* on the non-rotating sphere, while the two-frequency solutions are *relative equilibria* on the aligned non-rotating sphere in view of the relation (4.1). Note also that it is sufficient to consider only the orientation range $0 \leq \gamma \leq \pi$, as trajectories in the range $\pi < \gamma < 2\pi$ can be obtained by symmetry. In the region $0 \leq \gamma < \pi/2$, the rigid body moves in the same direction as the solid-body rotation (eastward), whereas in the region $\pi/2 < \gamma \leq \pi$ it moves in the opposite direction (westward). In what follows, we will look at the representative values $\gamma = \pi/4,\ \pi/2,\ 3\pi/4$.

(a) *One-frequency solutions*

To obtain necessary conditions for the one-frequency solutions on the rotating sphere, let $\dot{\boldsymbol{z}}_\alpha = \boldsymbol{\omega} \times \boldsymbol{z}_\alpha$ in (3.4), take the cross-product with $\Gamma_\alpha \boldsymbol{z}_\alpha$ and

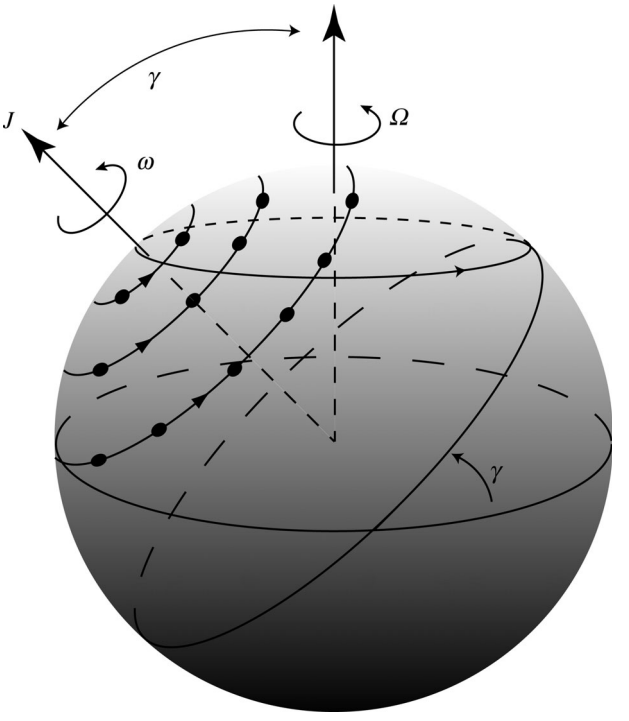

Figure 3. Rigid configurations on the rotating sphere are made up of rotations around two independent axes, with two independent frequencies. The vortices are *layered* on constant latitudinal planes that are perpendicular to the $\boldsymbol{J}$-axis.

sum on α

$$\sum_{\alpha=1}^{N} \Gamma_\alpha \boldsymbol{z}_\alpha \times (\boldsymbol{\omega} \times \boldsymbol{z}_\alpha) = \frac{1}{4\pi} \sum_{\alpha=1}^{N} {\sum_{\beta=1}^{N}}' \Gamma_\alpha \Gamma_\beta \frac{\boldsymbol{z}_\alpha \times (\boldsymbol{z}_\beta \times \boldsymbol{z}_\alpha)}{1 - \boldsymbol{z}_\alpha \cdot \boldsymbol{z}_\beta}$$
$$= \frac{1}{4\pi} \sum_{\alpha=1}^{N} {\sum_{\beta=1}^{N}}' \Gamma_\alpha \Gamma_\beta \frac{(\boldsymbol{z}_\beta - \boldsymbol{z}_\alpha (\boldsymbol{z}_\alpha \cdot \boldsymbol{z}_\beta))}{1 - \boldsymbol{z}_\alpha \cdot \boldsymbol{z}_\beta}$$
$$= \frac{1}{4\pi} \sum_{\alpha=1}^{N} {\sum_{\beta=1}^{N}}' \Gamma_\alpha \Gamma_\beta \boldsymbol{z}_\alpha = \frac{1}{4\pi} \left(S\tilde{\boldsymbol{J}} - \sum_{\alpha=1}^{N} \Gamma_\alpha^2 \boldsymbol{z}_\alpha \right), \tag{5.5}$$

where $S = \sum_{\alpha=1}^{N} \Gamma_\alpha$ is the total vorticity. Hence, a necessary condition for a fixed configuration ($\omega = 0$) on the aligned non-rotating sphere, i.e. a one-frequency rigid configuration on the rotating sphere is

$$S\tilde{\boldsymbol{J}} = \sum_{\alpha=1}^{N} \Gamma_\alpha^2 \boldsymbol{z}_\alpha. \tag{5.6}$$

It is interesting to note that the analogous condition for the existence of a fixed equilibrium configuration in the plane is given by

$$S^2 = \sum_{\alpha=1}^{N} \Gamma_\alpha^2, \tag{5.7}$$

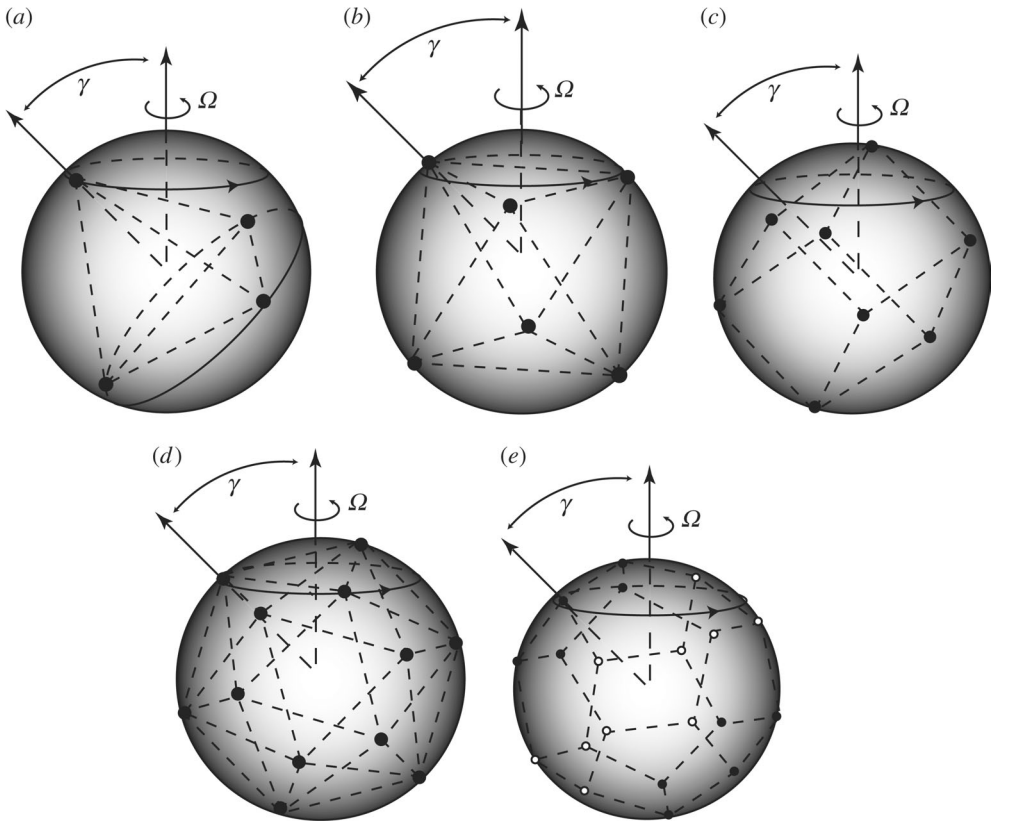

Figure 4. One-frequency rigid Platonic solids on the rotating sphere oriented at angle γ with respect to the north pole. (*a*) Tetrahedron (four equal vortices): one vortex is placed at the top, three are evenly spaced around the ring at the base; (*b*) octahedron (six equal vortices): four vortices are evenly spaced around the middle ring, one is placed at the top and one is placed at the bottom; (*c*) hexahedron (eight equal vortices): four vortices are evenly spaced around the top ring, four are evenly spaced around the bottom ring which is aligned with the top ring; (*d*) icosahedron (12 equal vortices): Five vortices are evenly spaced around the top ring, five vortices are evenly spaced on the bottom ring which is staggered with respect to the top ring, one vortex is placed at the top and one is placed at the bottom; and (*e*) dodecahedron (20 vortices): five equal strength vortices ($\Gamma_1 = \Gamma \sin\theta_1$) are evenly spaced along the outer top ring, five equal strength vortices ($\Gamma_1 = \Gamma \sin\theta_1$) are evenly spaced along the outer bottom ring staggered with respect to the outer top ring, five equal strength vortices ($\Gamma_2 = \Gamma \sin\theta_2$) are evenly spaced along the inner top ring, five equal strength vortices ($\Gamma_2 = \Gamma \sin\theta_2$) are evenly spaced along the inner bottom ring staggered with respect to the inner top ring.

as described in Aref *et al.* (2003). We show in figure 4, a family of one-frequency solutions on the rotating sphere given by the Platonic solids oriented at angle γ with respect to the axis of rotation. The details are described in the figure captions. Existence of these solutions as equilibria on the non-rotating sphere are described in Aref *et al.* (2003) and are special cases of some of the configurations studied in Lim *et al.* (2001) and Laurent-Polz (2002*a*,*b*). We note that a recent result of Kurakin (2004) shows that on the non-rotating sphere the tetrahedron, octahedron, and icosahedron are

nonlinearly stable, while the cube and dodecahedron are unstable. It is not clear whether the stability characteristics of these configurations are influenced by the application of $\mathcal{L}_Q^J(t)$.

(b) Two-frequency solutions

To obtain necessary conditions for two-frequency rigid rotations on the rotating sphere, take the scalar product of equation (5.5) with ω:

$$\sum_{\alpha=1}^{N} \Gamma_\alpha \boldsymbol{\omega}\cdot(\boldsymbol{z}_\alpha \times(\boldsymbol{\omega}\times\boldsymbol{z}_\alpha)) = \frac{1}{4\pi}\left(S\tilde{\boldsymbol{J}}\cdot\boldsymbol{\omega} - \sum_{\alpha=1}^{N}\Gamma_\alpha^2 \boldsymbol{z}_\alpha\cdot\boldsymbol{\omega}\right). \tag{5.8}$$

Then use the fact that

$$\boldsymbol{\omega}\cdot(\boldsymbol{z}_\alpha\times(\boldsymbol{\omega}\times\boldsymbol{z}_\alpha)) = (\boldsymbol{z}_\alpha\cdot\boldsymbol{z}_\alpha)(\boldsymbol{\omega}\cdot\boldsymbol{\omega}) - (\boldsymbol{\omega}\cdot\boldsymbol{z}_\alpha)^2. \tag{5.9}$$

Hence

$$\sum_{\alpha=1}^{N}\Gamma_\alpha(\|\boldsymbol{z}_\alpha\|^2\omega^2 - \omega^2\cos^2\theta_\alpha) = \frac{1}{4\pi}\left(S\tilde{\boldsymbol{J}}\cdot\boldsymbol{\omega} - \sum_{\alpha=1}^{N}\Gamma_\alpha^2\boldsymbol{\omega}\cos\theta_\alpha\right), \tag{5.10}$$

where $\boldsymbol{z}_\alpha\cdot\boldsymbol{\omega}=\omega\cos\theta_\alpha$. This gives a formula for the rotational frequency:

$$\omega\sum_{\alpha=1}^{N}\Gamma_\alpha\sin^2\theta_\alpha = \frac{1}{4\pi}\left(S\tilde{J}_z - \sum_{\alpha=1}^{N}\Gamma_\alpha^2\cos\theta_\alpha\right). \tag{5.11}$$

The analogous formula for rotating relative equilibria in the plane is

$$\omega\sum_{\alpha=1}^{N}\Gamma_\alpha|z_\alpha|^2 = \frac{1}{4\pi}\left(S^2 - \sum_{\alpha=1}^{N}\Gamma_\alpha^2\right), \tag{5.12}$$

described in Aref *et al.* (2003). Several examples of two-frequency solutions on the rotating sphere are described next.

(c) Dipole dynamics

A vortex dipole, shown in figure 5, is made up of two equal and opposite strength vortices, $\Gamma_1=\Gamma$, $\Gamma_2=-\Gamma$, $\theta_1=\theta$, $\theta_2=\pi-\theta$, $S=0$. The convention in this figure and those that follow is that black point vortices are positive (i.e. counterclockwise circulation) while white ones are negative (i.e. clockwise circulation). Formula (5.11) then becomes

$$\omega = \frac{\Gamma}{8\pi\cos\theta}. \tag{5.13}$$

It is a fundamental result that on a non-rotating sphere, a dipole follows the geodesic (i.e. great circle) that perpendicularly bisects the geodesic segment that connects the two vortices (Kimura 1999). Motion of a dipole on the sphere for the two-way coupled model was carried out in DiBattista & Polvani (1998) as an initial value problem in which the background vorticity (i.e. all vorticity not associated with the dipole) is placed initially in constant latitudinal strips in order to model solid-body rotation. Both point vortex dipoles and distributed

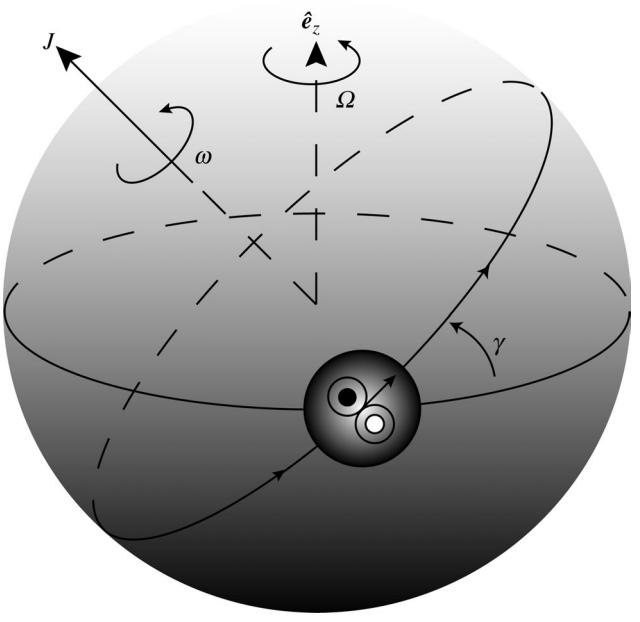

Figure 5. Dipole motion on a rotating sphere as a superposition of rotations about two axes with the two frequencies ω and Ω. Orientation angle is given by γ.

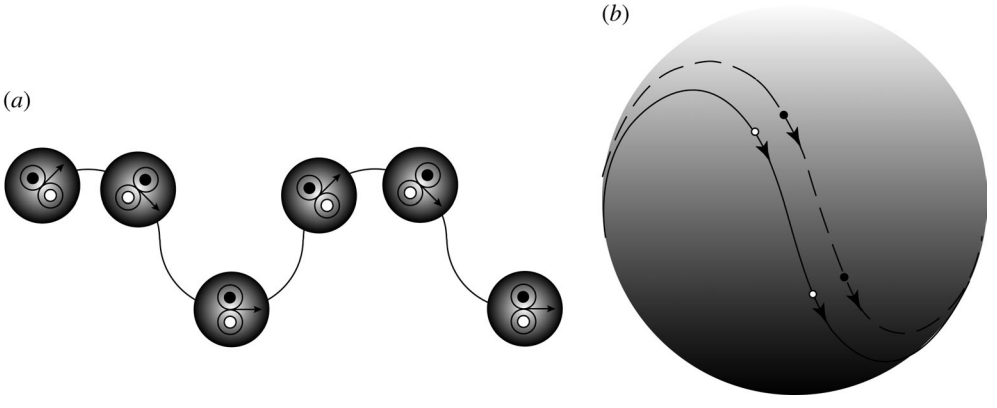

Figure 6. (*a*) Local (β-plane) wobbling mode (after Hobson 1991) associated with a vortex dipole and (*b*) global wobbling mode associated with a vortex dipole moving eastward on the sphere with orientation $\gamma = \pi/4$.

vortex dipoles were tracked numerically, showing, among other things, that dipoles no longer follow geodesic paths, but move on more complicated trajectories and in some instances can lose stability and tear apart. Because they only consider the case in which the $\boldsymbol{J}$ vector is aligned with the axis of rotation, they cannot distinguish between the effects of misalignment and the effect of coupling to the background field. Dipole motion on the β-plane in a one-way coupled model was studied by Hobson (1991) where two modes of motion, 'tumbling' and 'wobbling', were identified. Similarly, a one-way coupled β-plane

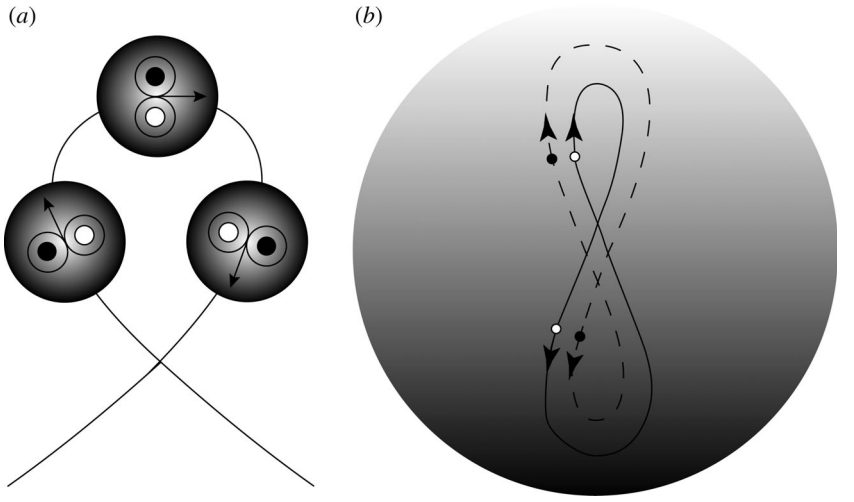

Figure 7. (*a*) Local (β-plane) tumbling mode (after Hobson 1991) associated with a vortex dipole and (*b*) global tumbling mode associated with a vortex dipole moving westward on the sphere with orientation $\gamma = 3\pi/4$.

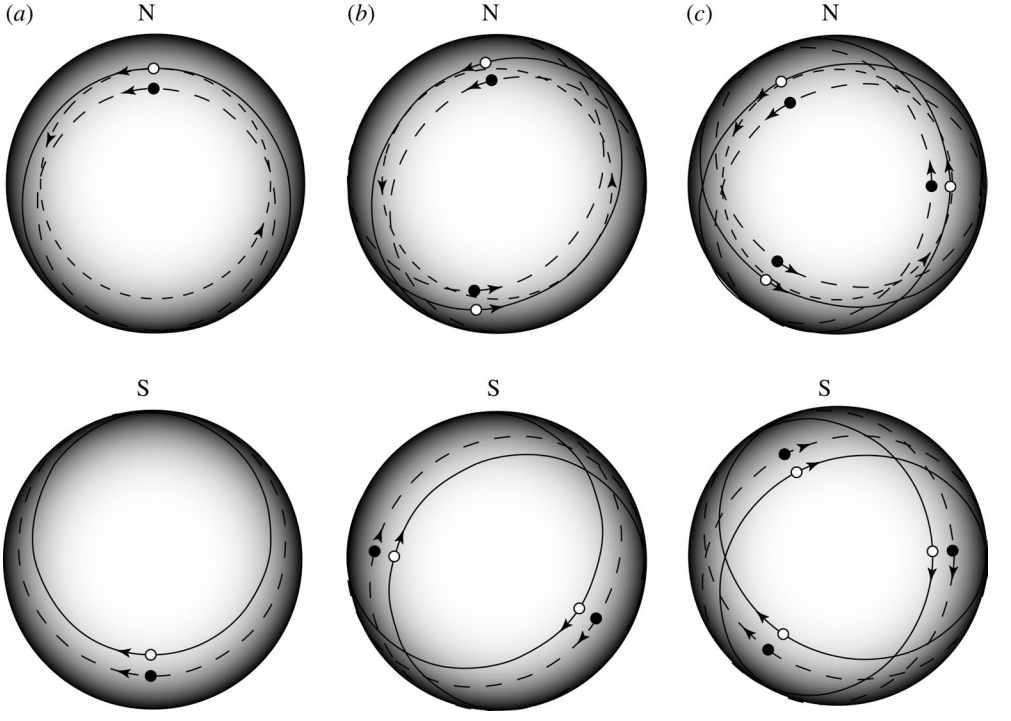

Figure 8. Dipole oriented at angle $\pi/4$, Northern and Southern Hemispheres. Trajectory of $\boldsymbol{J}$ vector is shown in the Northern Hemisphere (small dashed circle). (*a*) 1 : 1 frequency ratio; (*b*) 2 : 1 frequency ratio; and (*c*) 3 : 1 frequency ratio.

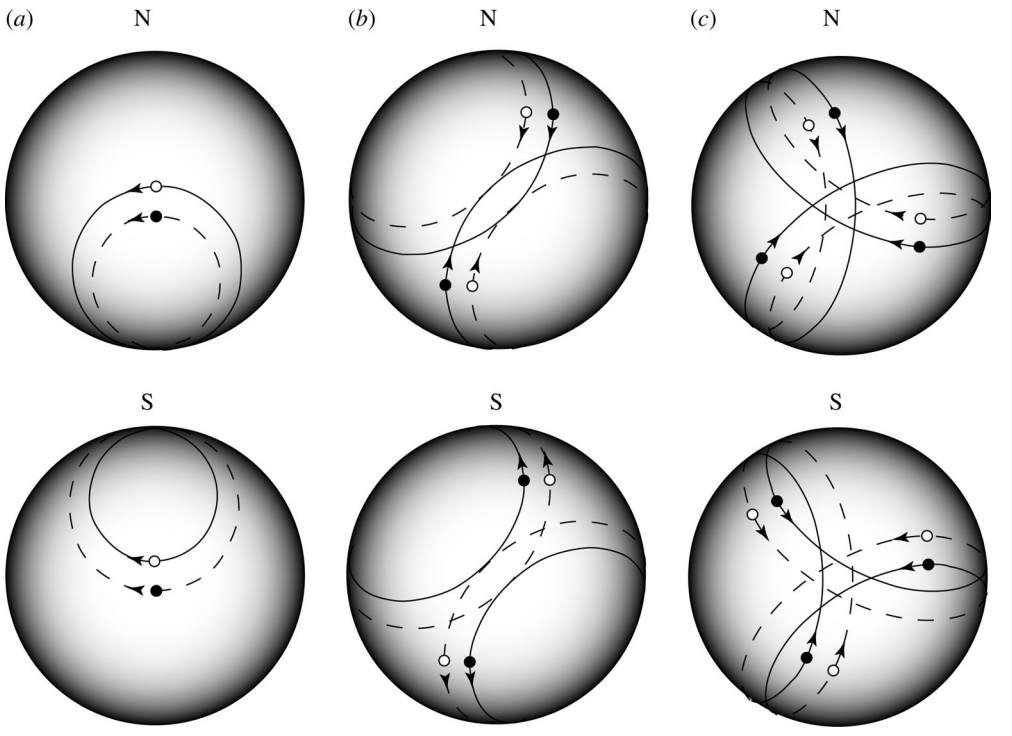

Figure 9. Dipole oriented at angle $\pi/2$, Northern and Southern Hemispheres. (*a*) 1 : 1 frequency ratio; (*b*) 2 : 1 frequency ratio; and (*c*) 3 : 1 frequency ratio.

model and the related modon solution were studied in Matsuoka & Nozaki (1992). Our general configuration is shown in figure 5 and is governed by three key parameters. The orientation angle, γ, measures the angle between the $\boldsymbol{J}$ vector and the axis of rotation around the North Pole. The frequency Ω is associated with the solid-body rotation, while frequency ω is associated with the dipole motion in the absence of rotation, i.e. its frequency around a great circle as given by formula (5.13). This is determined by the choice of vortex strengths, which we take as $\Gamma_1=1$ and $\Gamma_2=-1$ and the dipole separation (chord distance), which we take as $d=0.1=\sin\theta$. In all cases, we take the initial centre point of the dipole to lie on the equator at the front of the sphere (defined as longitude $\phi=0$), as shown in the figure. Figure 6 shows the β-plane wobbling mode of Hobson (1991) (figure 6*a*) and the corresponding 'global' wobbling mode (figure 6*b*) on the full sphere. The tumbling modes are shown in figure 7*a*,*b*. What distinguishes the two cases is the orientation angle. When $0<\gamma<\pi/2$, the dipole moves in the same direction as the rotation (eastward) and produces a wobbling trajectory. When $\pi/2<\gamma<\pi$, it moves initially opposite the direction of rotation (westward) and produces a tumbling trajectory.

Figures 8–10 show the dipole trajectories on the rotating sphere with orientation angles $\pi/4$, $\pi/2$ and $3\pi/4$, respectively. When the frequency ratio ω/Ω is rational, the motion is periodic. Cases with frequency ratios $\omega/\Omega=1$–3 are shown in the Northern and Southern Hemispheres, along with the trajectory of the $\boldsymbol{J}$ vector (dashed circle). Note that the cases $\gamma=\pi/4$ (figure 8) and $\gamma=3\pi/4$

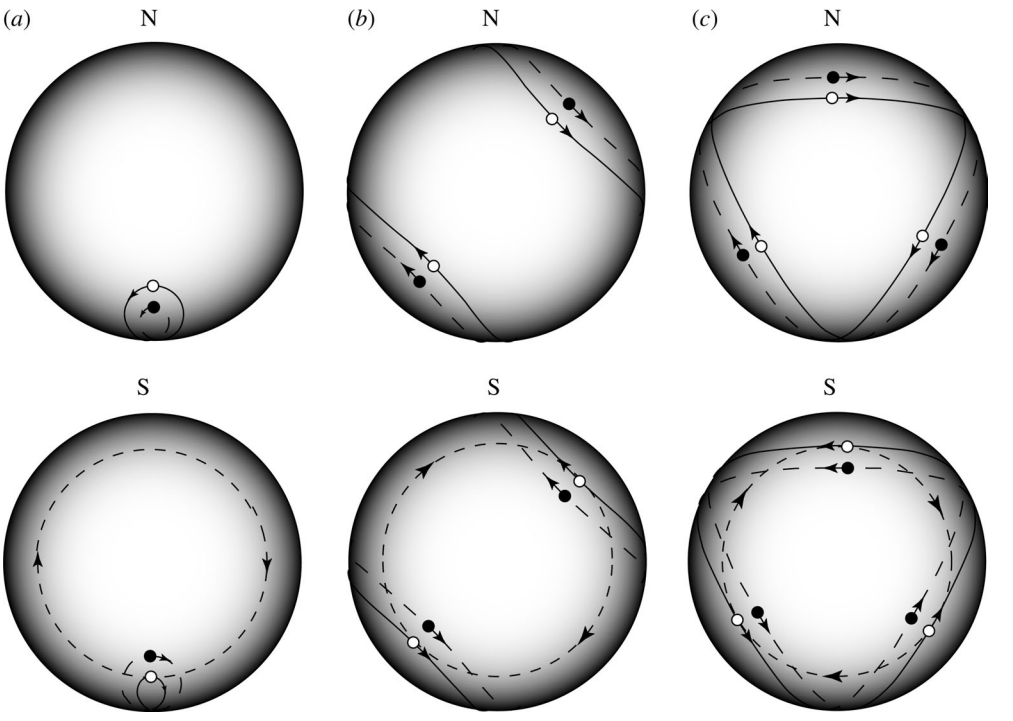

Figure 10. Dipole oriented at angle $3\pi/4$, Northern and Southern Hemispheres. Trajectory of $\boldsymbol{J}$ vector is shown in the Southern Hemisphere (small dashed circle). (*a*) 1 : 1 frequency ratio; (*b*) 2 : 1 frequency ratio; and (*c*) 3 : 1 frequency ratio.

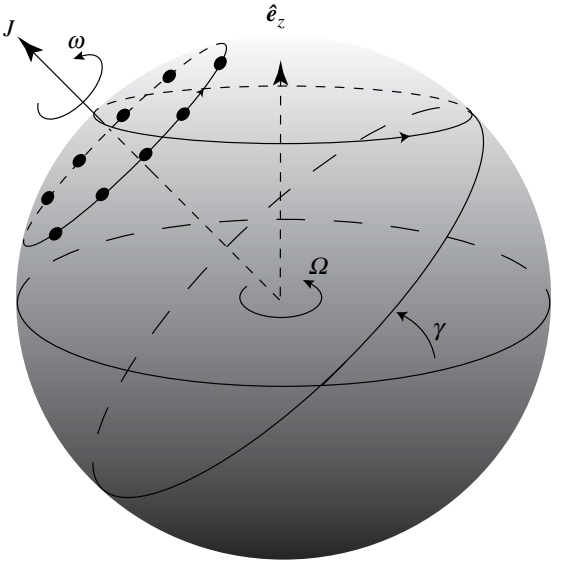

Figure 11. Equal strength vortices evenly spaced on a constant latitude cap perpendicular to the centre of vorticity vector on the rotating sphere.

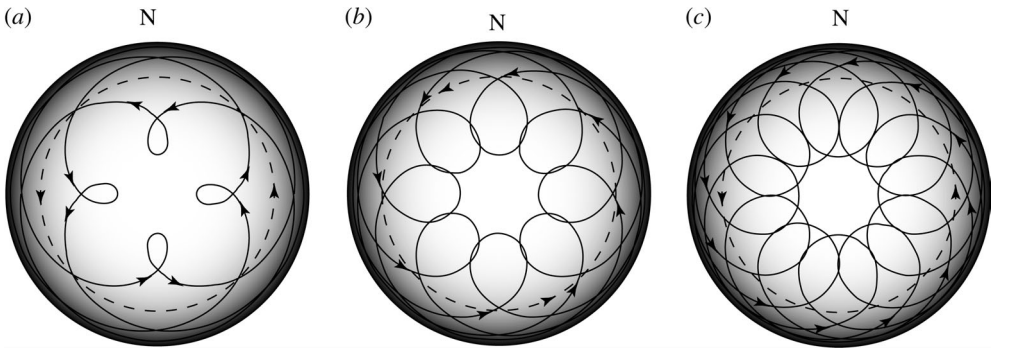

Figure 12. Four vortex ring oriented at angle $\pi/4$. Dashed circle shows the trajectory of the $\boldsymbol{J}$ vector. (*a*) 1 : 1 frequency ratio; (*b*) 2 : 1 frequency ratio; and (*c*) 3 : 1 frequency ratio.

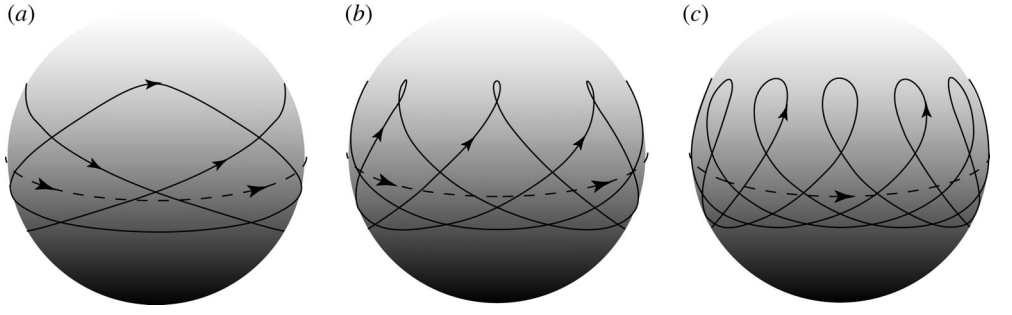

Figure 13. Four vortex ring oriented at angle $\pi/2$. Front of sphere is shown, dashed curve is the path of the $\boldsymbol{J}$ vector. (*a*) 1 : 1 frequency ratio; (*b*) 2 : 1 frequency ratio; and (*c*) 3 : 1 frequency ratio.

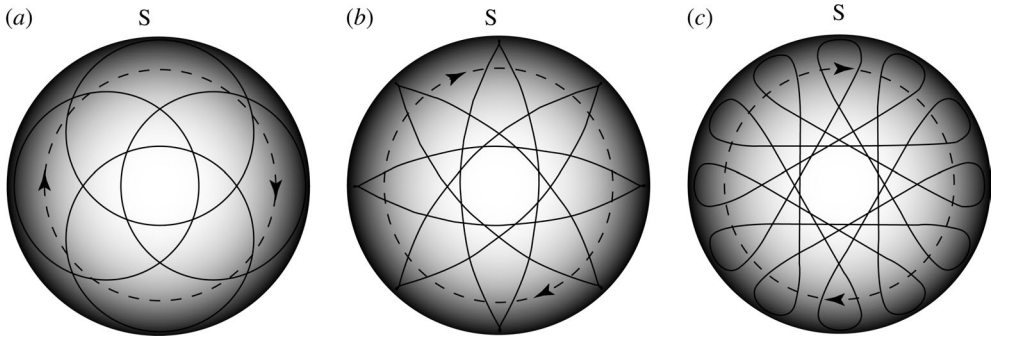

Figure 14. Four vortex ring oriented at angle $3\pi/4$, Southern Hemisphere only. Dashed curve is the path of the $\boldsymbol{J}$ vector. (*a*) 1 : 1 frequency ratio; (*b*) 2 : 1 frequency ratio; and (*c*) 3 : 1 frequency ratio.

(figure 10) are not related to each other via symmetries. In the first case, the dipole moves initially in the same direction as the solid-body rotation, while in the second case, it moves opposite to the direction of the solid-body rotation. When the frequency ratio is irrational, the long-time trajectory densely covers the available surface of the sphere allowed by the choice of the angle of orientation γ.

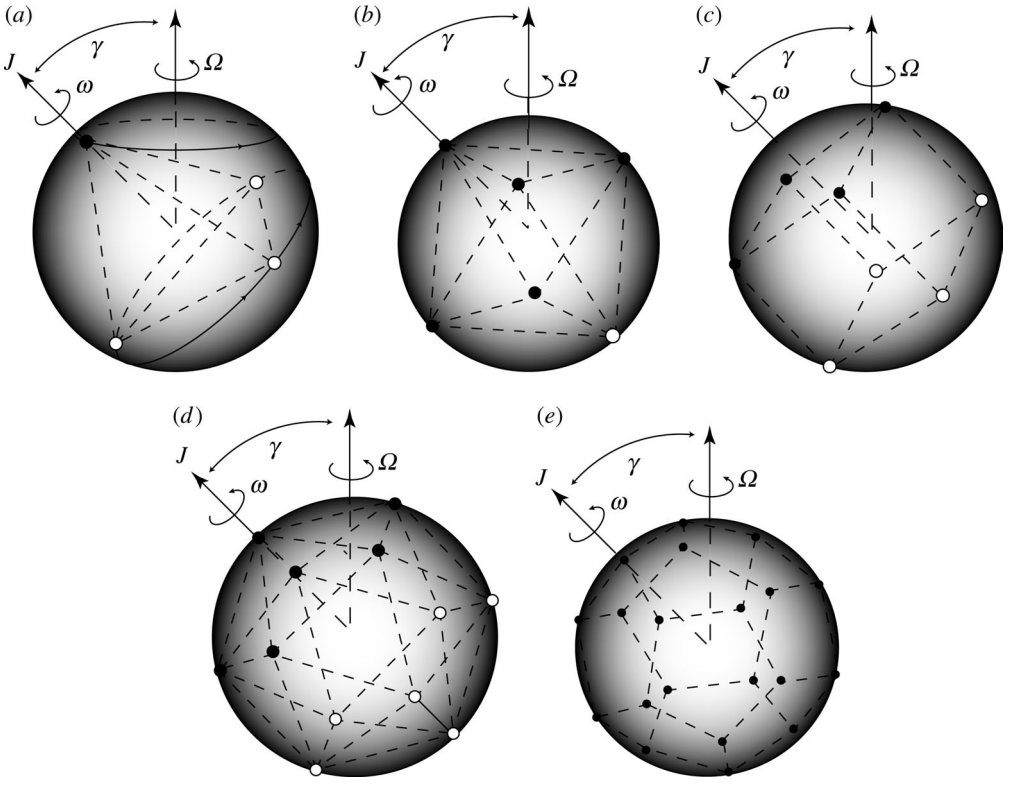

Figure 15. Same structures as in figure 4: (*a*) tetrahedron: Γ is placed at the top, $-\Gamma$s are evenly spaced around the bottom ring; (*b*) octahedron: Γs are evenly spaced around the middle ring, another is placed at the top, $-\Gamma$ is placed at the bottom; (*c*) hexahedron: Γs are evenly spaced around the top ring, $-\Gamma$s are evenly spaced around the bottom ring; (*d*) icosahedron: Γs are evenly spaced on the top ring, $-\Gamma$s are evenly spaced on the bottom ring, another Γ is placed at the top and $-\Gamma$ is placed at the bottom; and (*e*) dodecahedron: $\Gamma_1=\Gamma\sin\theta_1$ are evenly spaced along the outer top ring, $\Gamma_1=-\Gamma\sin\theta_1$ are evenly spaced along the outer bottom ring staggered with respect to the outer top ring, $\Gamma_2=\Gamma\sin\theta_2$ are evenly spaced along the inner top ring, $\Gamma_2=-\Gamma\sin\theta_2$ are evenly spaced along the inner bottom ring staggered with respect to the inner top ring.

(*d*) *Rings*

In the case of an isolated ring in which N-vortices of equal strength are arranged around a constant latitude cap perpendicular to $\boldsymbol{J}$ as shown in figure 11, we have $\Gamma_\alpha=\Gamma$, $\theta_\alpha=\theta$, $S=N\Gamma$ and $\tilde{J}_z=N\Gamma\cos\theta$, and formula (5.11) reduces to

$$\omega=\frac{\Gamma(N-1)}{4\pi}\,\frac{\cos\theta}{\sin^2\theta}. \tag{5.14}$$

The stability of such configurations on the non-rotating sphere (as well as ones with an additional polar vortex) have been studied in Polvani & Dritschel (1993), Cabral *et al.* (2003) and Laurent-Polz *et al.* (2004), and it is known that a single ring made up of N equal strength, evenly spaced point vortices is unstable for all co-latitudes if $N\geq 7$, whereas for $N<7$ there exist ranges of Lyapunov stability when the ring is near a pole. In general terms, an additional polar vortex can serve to stabilize or destabilize a ring; hence it stands to reason that the addition

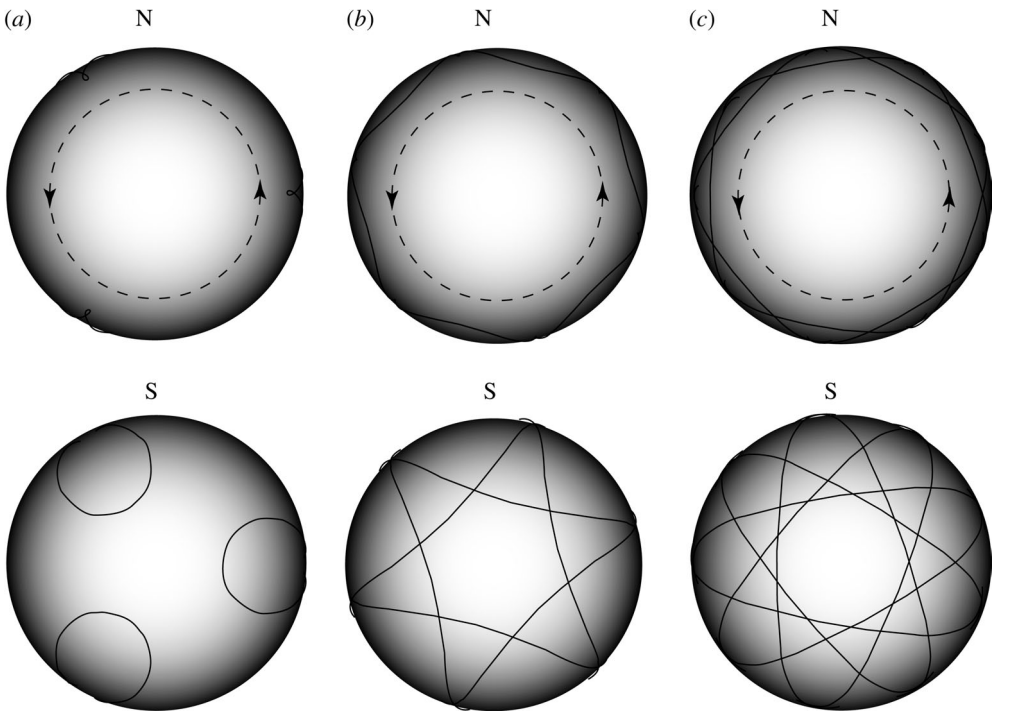

Figure 16. Two-frequency tetrahedron oriented at angle $\pi/4$, Northern and Southern Hemispheres. Dashed circle in the Northern Hemisphere marks the top of the configuration. (*a*) 1 : 1 frequency ratio; (*b*) 2 : 1 frequency ratio; and (*c*) 3 : 1 frequency ratio.

of solid-body rotation ($\Omega \neq 0$) may also alter the stability property of the ring, although this question has not been addressed. Figure 12 shows the vortex paths of a four-vortex ring with orientation angle $\pi/4$. The ring radius is $r=0.1$ and the trajectory of the $\boldsymbol{J}$ vector is shown as the dashed circle. Frequency ratios of 1 : 1, 2 : 1, and 3 : 1 are shown in the Northern Hemispheres as none of the vortices crosses the equator. Figure 13 shows the same ring oriented at angle $\gamma=\pi/2$. Trajectories corresponding to frequency ratios of 1 : 1, 2 : 1 and 3 : 1 are shown from the perspective of the front of the sphere. Figure 14 shows the same ring oriented at angle $\gamma=3\pi/4$. In this case, the ring's motion is opposite to the direction of rotation and gives different trajectories than those shown in figure 12. Frequency ratios of 1 : 1, 2 : 1, and 3 : 1 are shown in the Southern Hemispheres as none of the vortices crosses the equator.

(*e*) *Stacked rings: the Platonic solids*

More complex two-frequency rigid configurations on the rotating sphere are given by the Platonic solids shown in figure 15, where the vorticities have both positive and negative signs. Details are given in the figure captions. We show the evolution of a two-frequency tetrahedron in figures 16–18. In particular, figure 16 shows the trajectories of the four vortices making up a tetrahedral configuration oriented at angle $\gamma=\pi/4$. The dashed curve marks the trajectory of the top vortex, which in this case stays in the Northern Hemisphere. Frequency ratios of 1 : 1, 2 : 1 and 3 : 1 are shown. Figure 17 shows the same configuration oriented at

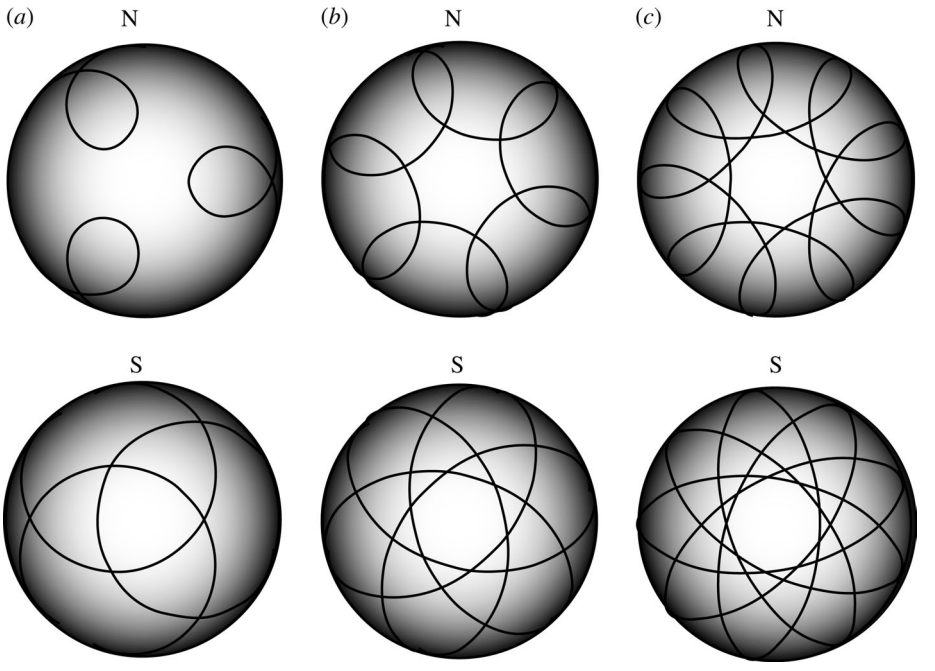

Figure 17. Two-frequency tetrahedron oriented at angle $\pi/2$, Northern and Southern Hemispheres. (*a*) 1 : 1 frequency ratio; (*b*) 2 : 1 frequency ratio; and (*c*) 3 : 1 frequency ratio.

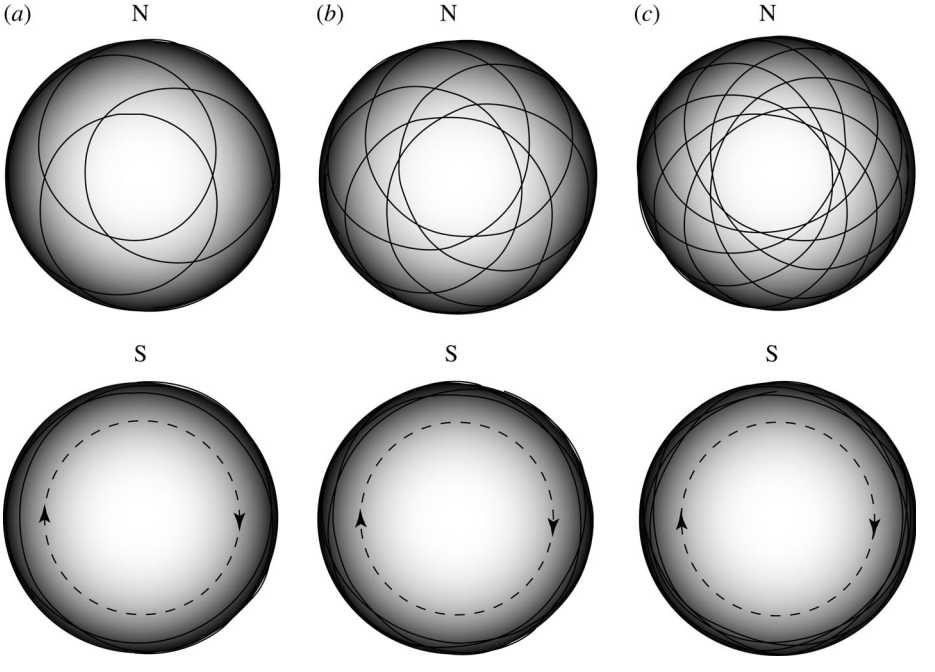

Figure 18. Two-frequency tetrahedron oriented at angle $3\pi/4$, Northern and Southern Hemispheres. Dashed circle in the Southern Hemisphere marks the top of the configuration. (*a*) 1 : 1 frequency ratio; (*b*) 2 : 1 frequency ratio; and (*c*) 3 : 1 frequency ratio.

angle $\gamma=\pi/2$ with frequency ratios of $1:1$, $2:1$ and $3:1$. The top of the tetrahedron in this case stays along the equator. Finally, figure 18 shows the tetrahedral configuration oriented at angle $\gamma=3\pi/4$ with frequency ratios $1:1$, $2:1$ and $3:1$. The top of the configuration now moves along the dashed circular curve shown in the Southern Hemisphere.

6. Discussion

The one-way coupled model (1.1) is useful for separating out two distinct effects that play a role in determining the long-time dynamics of vortices in fully coupled models such as those mentioned earlier. The misalignment of the $\boldsymbol{J}$ vector with the axis of rotation, on its own, can account for 'wobbling' and 'tumbling' dynamics, without the need for more complex explanations based on coupling to background fields. This point had not been made previously, hence none of the works that we are aware of keep track of the initial alignment of the $\boldsymbol{J}$ vector associated with the vortex field. The stability and ultimate fate of the rigid structures described in this paper, when fully coupled to the background field, would certainly be a topic worth pursuing.

This work is supported by the National Science Foundation grants NSF-DMS 9800797 and NSF-DMS 0203581.

References

Aref, H., Newton, P. K., Stremler, M. A., Tokieda, T. & Vainchtein, D. L. 2003 Vortex crystals. *Adv. Appl. Mech.* **39**, 1–79.

Bagrets, A. A. & Bagrets, D. A. 1997 Nonintegrability of two problems in vortex dynamics. *Chaos* **7**, 368–375. (doi:10.1063/1.166210)

Bogomolov, V. A. 1985 On the motion of a vortex on a rotating sphere. *Izv. Atmos. Ocean. Phys.* **21**, 298–302.

Borisov, V. A. & Lebedev, V. G. 1998 Dynamics of three vortices on a plane and a sphere II. *Regul. Chaotic Dyn.* **T.3**, 99–114. (doi:10.1070/rd1998v003n02ABEH000075)

Borisov, A. V. & Pavlov, A. E. 1998 Dynamics and statics of vortices on a plane and a sphere I. *Regul. Chaotic Dyn.* **T.3**, 28–38. (doi:10.1070/rd1998v003n01ABEH000059)

Cabral, H. E., Meyer, K. R. & Schmidt, D. S. 2003 Stability and bifurcations for the $N+1$ vortex problem on the sphere. *Regular Chaotic Dyn.* **8**, 259–282. (doi:10.1070/RD2003v008n03ABEH000243)

Chern S. J., 1991 Mathematical theory of the Barotropic model in geophysical fluid dynamics. Ph.D. dissertation, Cornell University.

DiBattista, M. T. 1997 Vortex pairs on the rotating sphere. Ph.D. thesis, Columbia University.

DiBattista, M. T. & Polvani, L. M. 1998 Barotropic vortex pairs on a rotating sphere. *J. Fluid Mech.* **358**, 107–133. (doi:10.1017/S0022112097008100)

Gill, A. E. 1982 Atmosphere–ocean dynamics. International Geophysics Series, vol. 30. New York: Academic Press.

Hobson, D. D. 1991 A point vortex dipole model of an isolated modon. *Phys. Fluids A* **3**, 3027–3033. (doi:10.1063/1.857846)

Jamaloodeen, M. 2000 Hamiltonian methods for some geophysical vortex dynamics models. Ph.D. thesis, University of Southern California.

Khushalani, B. 2004 Symplectic subcluster methods and periodic vortex motion on a sphere. Ph.D. thesis, University of Southern California.

Kidambi, R. 1999 Integrable point vortex motion on a sphere. Ph.D. thesis, University of Southern California.

Kidambi, R. & Newton, P. K. 1998 Motion of three point vortices on a sphere. *Physica D* **116**, 143–175. (doi:10.1016/S0167-2789(97)00236-4)

Kidambi, R. & Newton, P. K. 1999 Collision of three vortices on a sphere. *Il Nuovo Cimento* **22**, 779–791.

Kidambi, R. & Newton, P. K. 2000 Streamline topologies for integrable vortex motion on a sphere. *Physica D* **140**, 95–125. (doi:10.1016/S0167-2789(99)00233-X)

Kimura, Y. 1999 Vortex motion on surfaces of constant curvature. *Proc. R. Soc. A* **455**, 245–259. (doi:10.1098/rspa.1999.0311)

Klyatskin, K. V. & Reznik, G. M. 1989 Point vortices on a rotating sphere. *Oceanology* **29**, 12–16.

Kurakin, L. G. 2004 On nonlinear stability of the regular vortex systems on a sphere. *Chaos* **14**, 592–602. (doi:10.1063/1.1764432)

Laurent-Polz, F. 2002 Etude géométrique de la dynamique de N Tourbillons ponctuels sur une sphère. Ph.D. thesis, University of Nice.

Laurent-Polz, F. 2002*b* Point vortices on the sphere: a case of opposite vorticities. *Nonlinearity* **15**, 143–171. (doi:10.1088/0951-7715/15/1/307)

Laurent-Polz, F., Montaldi, J. & Roberts, M. 2004 *Stability of relative equilibria of point vortices on the sphere*. Preprint.

Lim, C. C., Montaldi, J. & Roberts, M. R. 2001 Relative equilibria of point vortices on the sphere. *Physica D* **148**, 97–135. (doi:10.1016/S0167-2789(00)00167-6)

Lim, C. C., Nebus, J. & Assad, S. M. 2003*a* Monte-Carlo and polyhedron based simulations. I. Extremal states of the logarithmic *N*-body problem on a sphere. *Discrete Contin. Dyn. Syst. B* **3**, 213–341.

Lim, C. C., Nebus, J. & Assad, S. M. 2003*b* A Monte-Carlo algorithm for the free and coaxial extremal states of the vortex *N*-body problem on a sphere. *Physica A* **328**, 53–96. (doi:10.1016/S0378-4371(03)00528-4)

Marsden, J. E., Pekarsky, S. & Shkoller, S. 1999 Stability of relative equilibria of point vortices on a sphere and symplectic integrators. *Il Nuovo Cimento* **22**, 793–802.

Matsuoka, C. & Nozaki, K. 1992 Point vortex model of a modon solution. *Phys. Fluids B* **4**, 551–558. (doi:10.1063/1.860254)

Nebus, J. 2003 Monte Carlo simulations, statistical mechanics, and ground states of the logarithmic potential. Ph.D. thesis, Rensselaer Polytechnic University.

Neven, E. C. 1993 Modons on a sphere. Ph.D. thesis, Eindhoven University of Technology.

Newton, P. K. 2001 *The N-vortex problem: analytical techniques*. Applied Mathematical Sciences Series, vol. 145. New York: Springer.

Newton, P. K. & Khushalani, B. 2002 Integrable decomposition methods and ensemble averaging for non-integrable *N*-vortex problems. *J. Turbulence*, pp. S1468–S5248.

Pekarsky, S. & Marsden, J. E. 1998 Point vortices on a sphere: stability of relative equilibria. *J. Math. Phys.* **39**, 5894–5907. (doi:10.1063/1.532602)

Polvani, L. M. & Dritschel, D. G. 1993 Wave and vortex dynamics on the surface of a sphere. *J. Fluid Mech.* **255**, 35–64.

Pullin, D. & Saffman, P. G. 1991 Long-time symplectic integration: the example of four-vortex motion. *Proc. R. Soc. A* **432**, 481–494.

Rowley, C. W. & Marsden, J. E. 2002 Variational integrators for degenerate Lagrangians with applications to point vortices. In *41st IEEE Conf. on Decision and Control,* paper 1521-15-27. Piscataway, NJ: IEEE.

Rowley, C. W., Marsden, J. E. & Newton, P. K. 2004 Variational integration schemes for the N-vortex problem. preprint.

Zhang, M. Q. & Qin, M. Z. 1993 Explicit symplectic schemes to solve vortex systems. *Comput. Math. Appl.* **26**, 51–56. (doi:10.1016/0898-1221(93)90073-5)

As this paper exceeds the maximum length normally permitted, the authors have agreed to contribute to production costs.